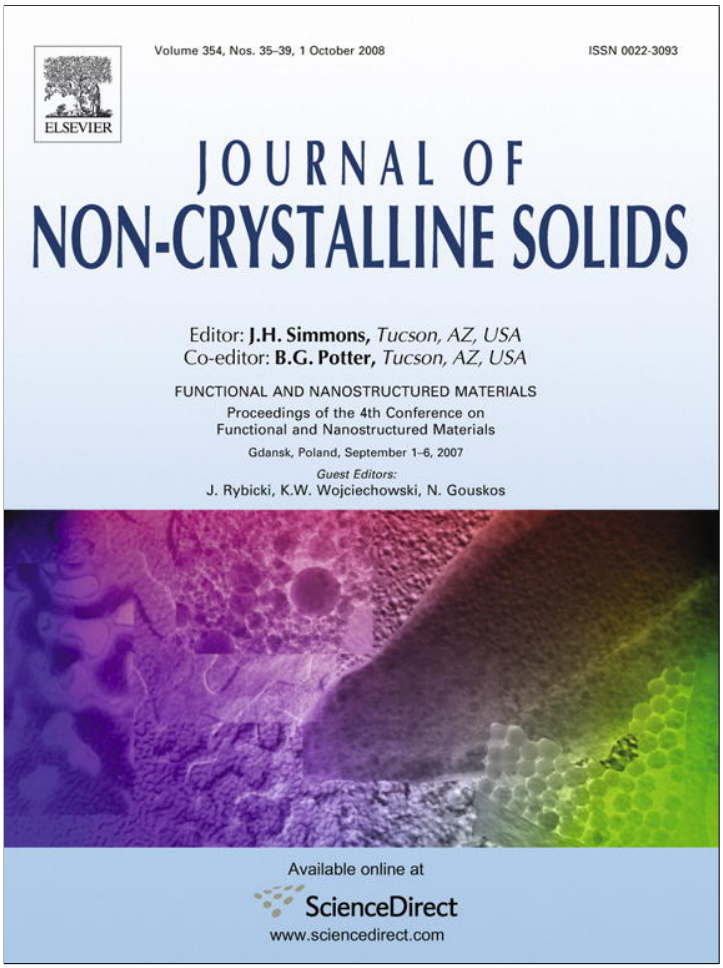

Journal of Non-Crystalline Solids 354 (2008) 4202–4210

Contents lists available at ScienceDirect

Journal of Non-Crystalline Solids

journal homepage: www.elsevier.com/locate/jnoncrysol

Low symmetry centers in $LiNbO_3$ doped with Yb and Er

S.M. Kaczmarek *, T. Bodziony

Institute of Physics, Szczecin University of Technology, Al. Piastów 17, 70-310 Szczecin, Poland

ARTICLE INFO

Article history:
Available online 11 August 2008

PACS:
76.30.-v
75.30.Hx
76.30.Kg

Keywords:
Optical properties
Defects

ABSTRACT

Electron paramagnetic resonance spectroscopy studies of $LiNbO_3$ single crystal doped with 1 wt% of Yb^{3+} and 0.1 wt% Er are reported. Additionally, Raman spectra of the following crystals are presented: $LiNbO_3$:Nd, Yb (0.5 wt%, 0.7 wt%), $LiNbO_3$:Nd, Mg (2 wt%, 6 wt%), and $LiNbO_3$:Er (0.3 wt%). Raman spectra have revealed bands in the 50–220 cm^{-1} range, suggesting the presence of localized phonons. The localized phonons may be considered as indirect evidence of local perturbations around Yb/Er ions, possibly due to formation of Yb/Er ion pairs. EPR spectra are interpreted basing on this presumption using a spin Hamiltonian for the Yb^{3+} dissimilar ion pairs. This model explains the observed spectral features, apparently due to the C_1 symmetry of Yb ions. In the case of the LN:Er sample, the angular dependence of EPR lines enabled distinguishing the presence of several non-equivalent centers. After deconvolution of the main EPR line into several Lorentzian components, the Er^{3+} center with the lowest C_1 point group symmetry was resolved and values of the $\boldsymbol{g}$ tensor were estimated.

1. Introduction

Due to its unique non-linear electric, magnetic and acousto-optic properties, lithium niobate, $LiNbO_3$ (LN), is one of the most extensively studied ferroelectric and electro-optic materials [1,2]. The space group of LN crystals is trigonal: $R3c$ (C_{3v}^6) [3,4]. The oxygen atoms of the LN structure are arranged in planar sheets forming a network of trigonally distorted octahedra, adjoined by walls forming chains along the crystallographic c-axis (i.e. the optical axis). The sequence of octahedra is repeated as {Nb, vacancy, Li}. Rare-earth (RE) impurity ions may occupy one of the four sites in LN: three octahedral sites, Li^+, Nb^{5+} or a cation vacancy, and the tetrahedral interstitial site. It has been demonstrated that trivalent RE ions occupy mostly Li^+ sites and are located off-center from the regular Li^+ positions towards the structural vacancy octahedral sites along the c-axis [1–4]. Thus, RE^{3+} ions may be distributed in crystallographically non-equivalent centers of this host, giving rise to different sets of optical transitions. Several experimental and theoretical studies have indicated that RE ions also occupy the Nb^{5+} sites in LN [5–7]. The structural analysis by Malovichko et al. [4] reveals that RE ions enter octahedral sites in $LiNbO_3$, which may exhibit not only the C_3 but also C_1 site symmetry.

LN is usually grown from congruent melt compositions with Li^+ to Nb^{5+} concentration ratios of the order of 0.945 ($x_c \approx 48.6\%$) giving rise to Li-deficient crystals that need intrinsic defects (antisites) for overall charge compensation. For a given RE^{3+} dopant ion, various crystallographically non-equivalent centers (NEC) may occur, whereas the relative concentration of such centers depends on stoichiometry (i.e. the Li/Nb concentration ratio). This result indicates that the nature of RE^{3+} centers in LN is directly related to the defects associated with the non-stoichiometric conditions. So, some of the above-mentioned properties may be drastically affected by the presence of impurities, growth conditions, or thermal treatment.

Single crystals of lithium niobate doped with ytterbium (LN:Yb) have been the subject of many studies concerning (i) energy transfer to Er^{3+} in up-conversion LN:Er, Yb lasers, (ii) self-doubling in their bulk, fibers and periodically poled structures, and (iii) laser cooling potential [5–7]. LN crystals doped with erbium (LN:Er) have been widely studied due to the development of Er^{3+} amplifiers in optical fibers and as an active medium for the Er^{3+} frequencies [8–10].

The present paper is a continuation of previous papers on EPR and optical measurements of single doped LN:Yb [11] and LN:Er [12] crystals and single LN:Yb, Pr [13] crystals. We have found new paramagnetic centers with the lowest C_1 point group symmetry in LN:Yb and LN:Er single crystals. The unusual behavior of the temperature dependence of the EPR lines' intensity and line width have been explained assuming the existence of Yb–Yb and/or Er–Er ion pairs in single crystals.

Details of the sample are given and general experimental conditions are outlined in Section 2. Raman spectroscopy studies are briefly discussed in Section 3.1. Analysis of the EPR spectra and their temperature dependence is carried out in Section 3.2. Optical spectroscopy is analyzed in Section 3.2.1 to put the EPR results into perspective. Non-equivalent crystallographic sites of low C_1 point

* Corresponding author. Tel.: +48 914494887; fax: +48 914494181.
E-mail address: skaczmarek@ps.pl (S.M. Kaczmarek).

0022-3093/$ - see front matter © 2008 Elsevier B.V. All rights reserved.
doi:10.1016/j.jnoncrysol.2008.06.092

group symmetry are analyzed in Section 3.3. Since changes of the EPR line profiles may also be related to several inequivalent Er^{3+}/Yb^{3+} centers, arguments against this alternative explanation are discussed. Some of the results discussed in Section 3 have been presented earlier (optical spectroscopy, angle dependencies [11–13]) and the paper may thus be treated as an invited paper, but most of them are shown here for the first time (analysis of the EPR lines' temperature dependences). A summary and conclusions can be found in Section 4.

2. Samples and experimental details

$LiNbO_3$ single crystals doped with Yb^{3+} and Er^{3+} were grown along the *c*-axis from the congruent melt by the Czochralski method at the Institute of Electronic Materials Technology (IEMT). The Yb concentration was 1% (sample #1), Er – 0.1% (sample #5) of the melt's molar fractions: Nb_2O_5 (4 N purity) from Johnson–Matthey and Li_2CO_3 (4 N purity) from IEMT were used as starting materials. Yb_2O_3 and Er_2O_3 were added to the charge of congruent melt with the Li/Nb ratio of 0.94 prior to synthesis at elevated temperatures. A more detailed description of the applied growth process is presented elsewhere (see [14]). The following crystals were also investigated: (#2) $LiNbO_3$:Nd, Yb (0.5 wt%, 0.7 wt%), (#3) $LiNbO_3$:Nd, Mg (2 wt%, 6 wt%) and (#4) $LiNbO_3$:Er (0.3 wt%).

The *X*(*YZ*)*Y* Raman spectra were recorded for samples #2–4 for the type A and E modes with a resolution of 0.56 cm^{-1} at the Institute of Low Temperature and Structural Research, Wroclaw. A SPEX 1403 Raman spectrometer was employed with right-angle scattering geometry and a 488 nm line of an Ar^+ laser.

The LN samples used for electron paramagnetic resonance (EPR) studies were cut out from the bulk sample oriented at room temperature using the X-ray diffraction method (XRD) and polished. The samples had the form of parallel plates 3.1 × 2.7 × 1.5 mm in dimensions with surfaces perpendicular to the *c*-axis determined from XRD. The laboratory axis system (*XYZ*) was chosen as follows: the *Z*-axis was taken along the crystallographic (i.e. optical) *c*-axis, the *X*-axis – along the one of the crystallographic *a*-axes, and the *Y*-axis as perpendicular to the *Z*- and *X*-axes. EPR spectra were recorded at the Institute of Physics, Szczecin University of Technology (SUT), Poland, using a Bruker E 500 X-band spectrometer ($\nu \sim 9.4$ GHz) with 100 kHz field modulation equipped with an Oxford flow cryostat for measurements at temperatures from that of liquid nitrogen down to 4 K. The samples were mounted on a goniometer to measure the angular dependence of their spectra.

3. Results and discussion

3.1. Raman spectra

All the investigated crystals were low-doped with RE ions. Nevertheless, we have been able to make some predictions of the RE pairs appearing in the crystals from the EPR measurements. The aim of the Raman spectra investigation was finding evidence of the presence of RE pairs in the crystals. The Raman spectra presented in Fig. 1 suggest the following modes in the 20–1200 cm^{-1} range: 152 cm^{-1} $E(TO_1)$ (Fig. 1(a)), 254 cm^{-1} $A_1(TO_1)$, 274 cm^{-1} $A_1(TO_2)$ (Fig. 1(b)), 331 cm^{-1} $A_1(TO_3)$ (Fig. 1(c)), 583.1 cm^{-1} $E(TO_8)$ and 630.2 cm^{-1} $A_1(TO_4)$ (Fig. 1(d)). The $E(TO_1)$, $A_1(TO_1)$ and $A_1(TO_2)$ modes are significantly affected by doping (broadening and shifting). Moreover, additional 100 cm^{-1}, 193 cm^{-1} and 238 cm^{-1} modes are recognizable due to the extrinsic doping and co-doping (see e.g. [18]). As compared with Mouras et al. [18], we have recognized two new bands, at 100 cm^{-1} and 238 cm^{-1}. We believe the former to be responsible for the presence of RE pairs. The latter, while also observed by Mouras et al., was not previously assigned to a particular vibrational mode. Having observed this band mainly in the co-doped LN crystals, we attributed it to co-doping and/or pair presence.

Phonons of the localized type appear to be responsible for all these modes. This suggests that an Yb/Er ion or another RE ion may be located near at least some of the Yb^{3+}/Er^{3+} ions, possibly forming pairs with them and thus perturbing the isolated Yb^{3+}/Er^{3+} ion spectra.

3.2. EPR spectroscopy measurements

Yb^{3+} and Er^{3+} are Kramers ions with an effective electron spin of all isotopes of $S_{eff} = 1/2$. In order to put the EPR results in perspec-

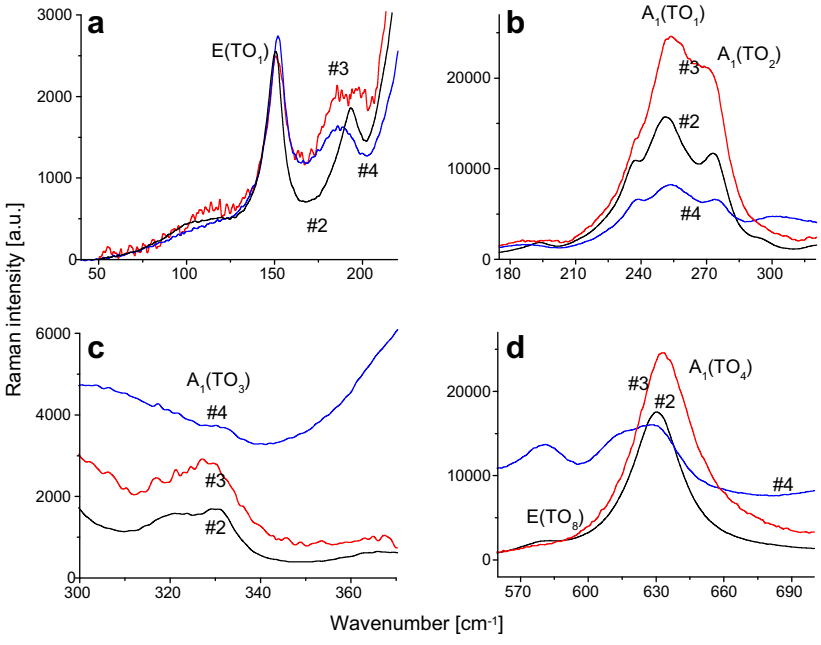

Fig. 1. Raman spectra recorded for (#2) $LiNbO_3$:Nd, Yb (0.5 wt%, 0.7 wt%), (#3) $LiNbO_3$:Nd, Mg (2 wt%, 6 wt%) and (#4) $LiNbO_3$:Er (0.3 wt%).

tive, we should analyze conclusions achievable using optical spectroscopy methods.

3.2.1. Optical spectra

In LN, Yb^{3+} and Er^{3+} ions usually occupy the Li^{+} sites with C_3 symmetry [16].When isolated Yb^{3+} ions occurred in LN at sites with lower, C_1 symmetry, no distinct features due to low symmetry (e.g. splitting of levels) could be observed in the crystal field (CF) energy levels [15]. No further splitting due to the crystal field of lower symmetry is allowed by the group theory, since the C_3 symmetry CF levels are the Stark doublets that can only be split by an external magnetic field.

The optical spectra of the $LiNbO_3$:Yb^{3+} single crystal (#1) have been reported in [15]. No pair absorption or emission of Yb^{3+} ions has been observed due to low concentration of impurity ions. Nevertheless, the main Yb^{3+} 979.7 nm line has a maximum at about 473 K, corresponding to energy equal to about 100 cm^{-1}. The shape of the temperature dependence of this line suggests the presence of localized phonons near Yb^{3+} ions, which may be due to other Yb^{3+} ions in the vicinity [11,15]. Moreover, our unpublished results suggest a shift of the 2866 nm centered OH^{-} absorption band towards shorter wavelengths (compared with 2873 nm for pure LN) and a complex asymmetric shape confirming the presence of a complex defect structure near Yb^{3+} ions.

The optical spectra of LN:Er^{3+} single crystal have been reported in [8]. The crystal's gamma-induced absorption spectrum has a few sharp peaks corresponding to changes in the absorption intensity of erbium ions [12]. The peaks' changes were not monotonic in the range of erbium absorption. Such additional absorption behavior is characteristic for single crystals in which the presence of pairs of dopant ions is suspected. The shape of induced absorption suggests recharging an Er^{3+} ion from a pair due to Compton electron capturing, previously reported for fluoride single crystals doped with Yb^{3+} [17]. As in the case of ytterbium doping of an LN single crystal, only some variation in the energy level values (and possibly in their sequence) may be expected due to low-symmetry CF components.

This makes it extremely difficult to distinguish any low symmetry effects in the optical spectra or to identify the CF transitions from Yb^{3+}/Er^{3+} ions located at the various possible low-symmetry sites.

3.2.2. EPR angle dependencies

3.2.2.1. LN:Yb. Theoretically, signals originating at the temperature of liquid helium from isolated Yb^{3+} ions in an LN host may manifest themselves as a single central line originating from the fine-structure transitions due to the ^{even}Yb isotope (^{170}Yb, natural abundance: NA = 69.6%) with zero nuclear spin, $I = 0$, and/or as two hyperfine transitions distributed about a central line due to the ^{171}Yb odd isotope (NA = 19.3%) with $I = 1/2$, and/or as six hyperfine transitions distributed about a central line due to the ^{173}Yb odd isotope (NA = 16.1%) with $I = 5/2$ [19].

However, the observed EPR spectra of the LN:Yb^{3+} single crystal also manifest more sophisticated features suggesting the existence of magnetically coupled pairs of Yb^{3+} ions in the LN crystal. The coupled pairs of Yb ions may be represented in the EPR spectrum as similar or dissimilar ion pairs. The EPR spectra of similar ion pairs are characterized by a pattern of two lines of similar intensity, whereas those of dissimilar pairs are characterized by a four-line pattern, with the two middle lines much more intense than the two satellite lines. Some of the observed EPR spectra reveal a recognizable four-line pattern characteristic for EPR spectra originating from dissimilar RE ion pairs [20,21].

Representative EPR spectra of the LN:Yb^{3+} (1 wt%) sample [11,22] taken at various angles in the *ZX* plane containing the crystal's *c* (*Z*)-axis are presented in Fig. 2. The angular dependence of

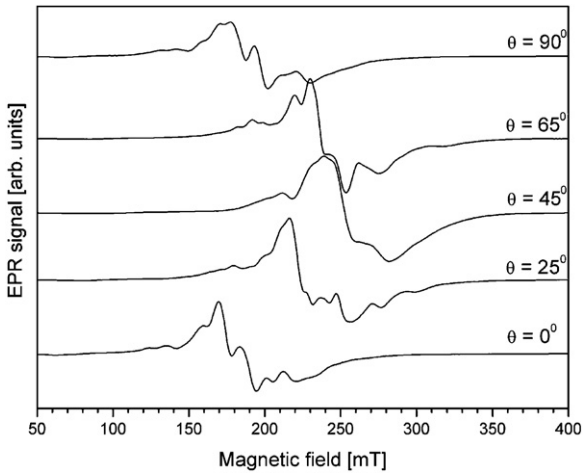

Fig. 2. Sample EPR spectra for a Yb^{3+}-doped LN crystal measured at 6–8 K in the *ZX* plane containing the crystal's *c*-axis ($\theta = 0^{\circ}$ denotes the *Z*-axis).

EPR lines indicates that the observed spectra are a result of superposition of signals that may arise from either magnetically inequivalent paramagnetic centers of the same type or crystallographically distinct centers of the same or different type [19]. Moreover, the angular dependence of EPR lines exhibits behavior characteristic for sites of very low symmetry. When the direction of magnetic field rotates away from the *Z*-axis, the lines move towards higher values of the magnetic field until they change direction towards lower values past 45° [23]. We have not observed EPR spectra exhibiting axial symmetry.

Based on the pair model, which assumes pair interaction through space and not through bonds, the actual mechanism responsible for the magnetic interactions of Yb–Yb ion pairs is ascribed to the magnetic dipole–dipole interaction [20,21]. A computer program was used to compute parameters of the spin Hamiltonian for a model of dissimilar RE ion pairs and a negative isotropic parameter (interaction constant) of $J = -0.028 \pm 0.001$ (cm^{-1}) was obtained, indicating antiferromagnetic coupling between the Yb^{3+}–Yb^{3+} pair ions at 8 K [22]. It also follows from our calculations that the pair axis is not parallel to the *c*-axis, ytterbium pairs thus exhibiting low C_1 symmetry [4].

3.2.2.2. LN:Er. The spin Hamiltonian characterizing EPR spectra of all isotopes of Er^{3+} ions with the effective spin of $S_{eff} = 1/2$ can be written as a sum of the electronic Zeeman and hyperfine terms [21]:

$$H = \mu_B \mathbf{S} \cdot \mathbf{g} \cdot \mathbf{B} + \mathbf{S} \cdot \mathbf{A} \cdot \mathbf{I}, \quad (1)$$

where μ_B is the Bohr magneton, $\mathbf{S}$ is the electron spin, $\mathbf{I}$ is the nuclear spin of paramagnetic centers, $\mathbf{B}$ is the external magnetic field, while $\mathbf{g}$ and $\mathbf{A}$ are anisotropic and generally non-coincident tensors, respectively characterizing Zeeman and hyperfine interactions.

The EPR spectra of Er-doped single LN crystals at the temperature of liquid helium (see Fig. 3) have a strong central line corresponding to the fine-structure transition of ^{even}Er isotopes ($\mathbf{I} = 0$, no nuclear magnetic moments for ^{166}Er, ^{168}Er and other even isotopes, natural abundance 77.06%) and eight hyperfine transitions distributed about the main fine transition corresponding to the nuclear spin of ^{167}Er isotopes ($\mathbf{I} = 7/2$, natural abundance 22.94%) [19].

Fig. 3 presents the angular dependence of EPR lines for the Er^{3+}-doped LN crystal measured at 8 K in the plane containing the crystal's *c*-axis ($\theta = 0^{\circ}$ defines the *Z*-axis). When the magnetic field's direction is rotated away from the *Z*-axis, the EPR line (fine transi-

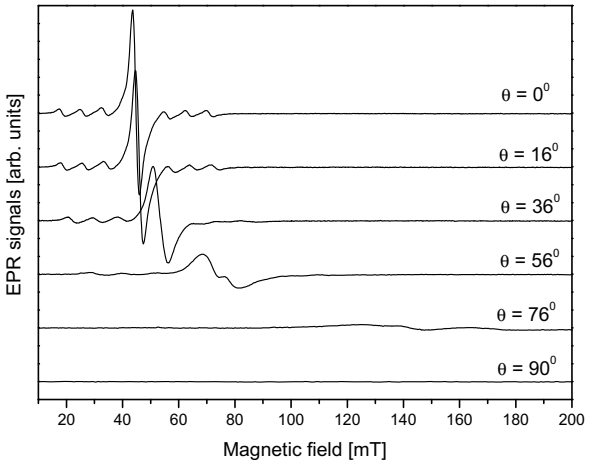

Fig. 3. Angular dependence of EPR lines of a LN:Er^{3+} crystal measured at 8 K in the plane containing its *c*-axis ($\theta = 0°$ defines the *c*-axis).

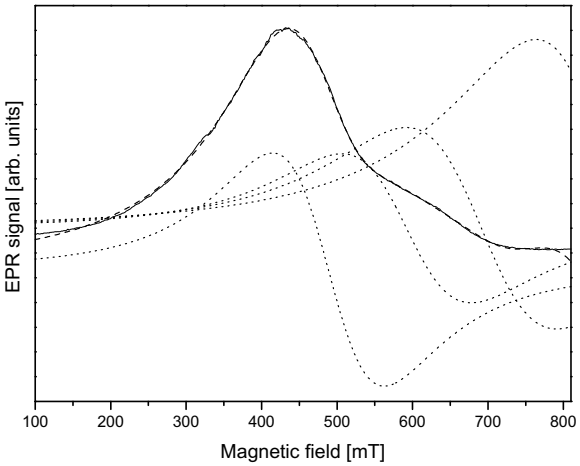

Fig. 5. The main line of an LN:Er^{3+} crystal's EPR spectrum measured for angle $\varphi = 80°$ at $T = 8.6$ K (solid line), the four constituent Lorentzian lines (dotted lines) and the sum of the constituent lines (dashed line).

tion) clearly moves towards higher values of magnetic field. When the θ angle between the direction of magnetic field and the crystal's *c*-axis exceeds 36°, the fine line originating from even erbium isotopes (^{even}Er) is split into several lines. The split is more pronounced when the direction of magnetic filed approaches the *XY* plane perpendicular to the crystal's *Z*-axis.

The behavior of EPR lines shown in Fig. 4 in a plane perpendicular to the *z*-axis (optical *c*-axis) is more complex. The strong central line is split into several lines, some of them moving in the range between 200 and 1400 mT. The broad strong line observed at about 400 mT seems to be a superposition of several lines originating from different paramagnetic centers, moving during the sample's rotation. In order to describe the behavior of the broad strong line (fine-structure transition), we have performed its deconvolution into four Lorentzian lines, the reasonable minimum number.

A sample of the main EPR line's deconvolution into four constituent Lorentzian lines is shown in Fig. 5: the EPR spectrum of an LN:Er^{3+} crystal measured in the plane perpendicular to the crystal's *c*-axis ($\varphi = 80°$) at a temperature of $T = 8.6$ K (solid line), the four constituent Lorentzian lines (dotted lines) and the sum of these lines (dashed line). The line sum of the constituent lines reproduces the shape of the observed EPR line very closely. The differences appear only in the magnetic field, just above 100 mT and just below 810 mT (see Fig. 5).

The angular dependence of the LN:Er^{3+} crystal's EPR spectra measured in the 6–9 K temperature range in the plane perpendicular to the crystal's *c*-axis is shown in Fig. 6. A fitting procedure was used to deconvolute the main and strongest EPR line, but additional EPR lines can be observed in some directions (see Fig. 4) that move towards higher magnetic field, up to 1200 mT. The resonance fields of these EPR lines are also marked in Fig. 6. As can be seen in Fig. 6, some of the marked points are arranged in a characteristic pattern, a fingerprint of the NEC point group symmetry. We used these points to calculate the spin-Hamiltonian parameters (Eq. (1)) and draw the fitted line by applying the EPR–NMR program [24].

The lines with the best fit parameters are shown in Fig. 6 as solid lines. Three kinds of lines can be distinguished, as the six lines marked in Fig. 6 form three pairs of lines and the positions of the two lines of each pair are indistinguishable. The angular dependence of all Er^{3+} centers in the LN:Er^{3+} single crystal in all three perpendicular planes is presented in Fig. 7. The behavior of the resonance line positions of Er^{3+} centers observed in Fig. 7 corresponds

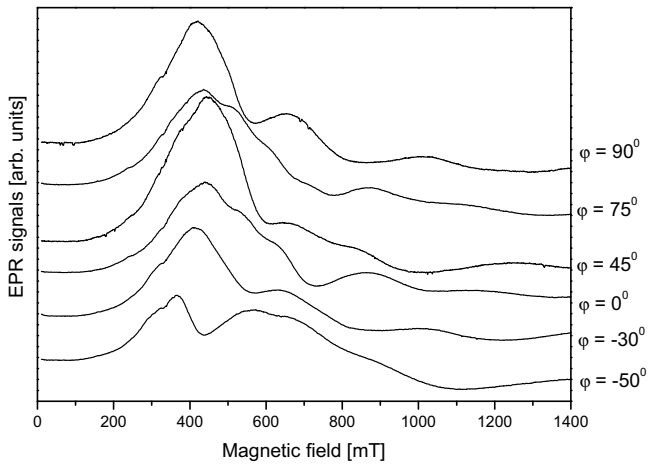

Fig. 4. Angular dependence of EPR lines of a LN:Er^{3+} crystal measured at 8 K in the plane perpendicular to its *c*-axis ($\varphi = 0$ defines the *x*-axis).

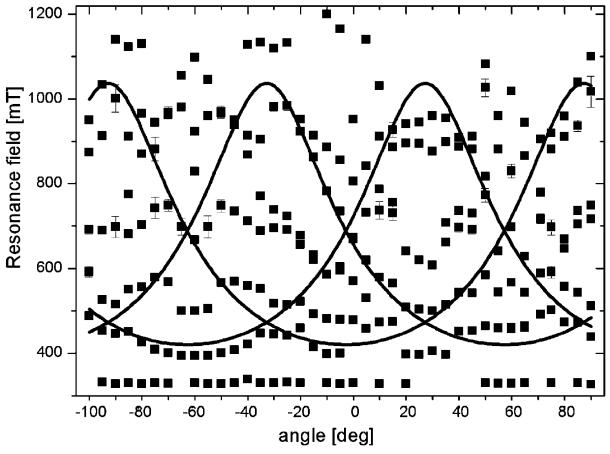

Fig. 6. Angular dependence of the EPR spectra of an LN:Er^{3+} crystal measured at 8 K in the plane perpendicular to the crystal's *c*-axis, with fitting lines marked. The black squares mark the positions of deconvoluted Lorentzian-shaped lines and measured EPR lines from the spectrum (with error bars). The lines' positions have been calculated using the spin Hamiltonian (EPR–NMR program [24]).

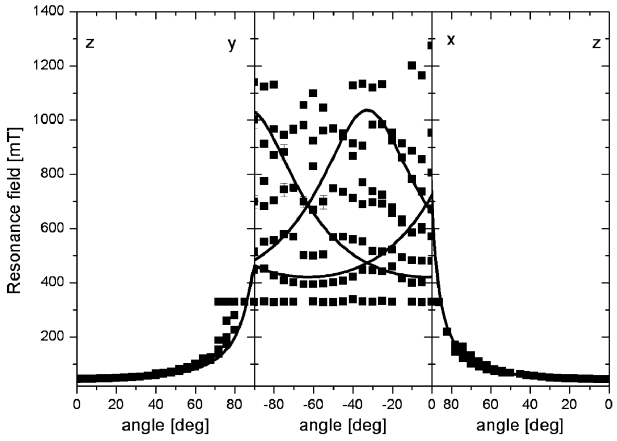

Fig. 7. Angular dependence of the EPR spectra of an LN:Er^{3+} crystal measured at 8 K in all three perpendicular planes. The black squares mark the positions of deconvoluted Lorentzian-shaped lines and measured EPR lines from the spectrum (with error bars). Lines are calculated using the spin Hamiltonian (EPR–NMR program [24]).

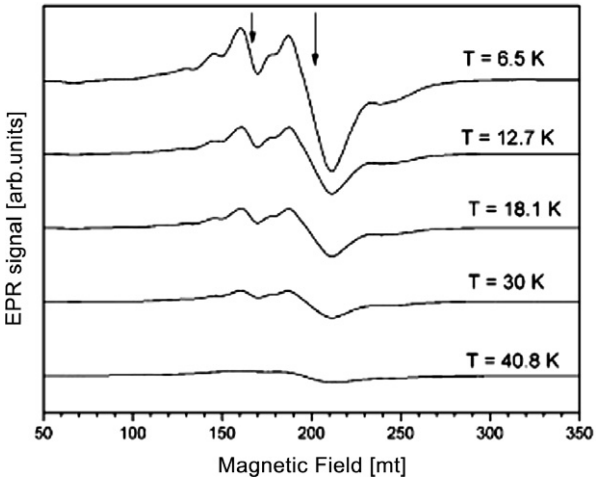

Fig. 8. Sample EPR spectra of an LN:Yb^{3+} crystal measured at various temperatures and a fixed angle ($\theta = 10°$) in the *ZY* plane containing the crystal's *c*-axis. Arrows indicate lines 1 (left arrow) and 2 (right arrow) chosen for detailed analysis.

to the specific features of low-symmetry centers in lithium niobate [25]. The best fit parameters are as follows:

$$g_{xx} = 0.546 \pm 0.110, \quad g_{yy} = 1.356 \pm 0.024,$$
$$g_{zz} = 15.093 \pm 0.074,$$
$$g_{xy} = -0.293 \pm 0.032, \quad g_{xz} = -0.700 \pm 0.084,$$
$$g_{yz} = 0.456 \pm 0.076.$$

The calculated values of the g_{zz} and g_{xx} parameters are comparable with the corresponding parameters reported in Ref. [26]. The angular dependence shown in Fig. 7 has a very weak EPR line which is not moving in the plane perpendicular to the *Z*-axis and is visible in the same position at about ~329 mT in an angle range close to 90° in the other two planes. The calculated $\boldsymbol{g}$ parameter for this line equals $\boldsymbol{g} = 2.05 \pm 0.02$ and is very close to the $\boldsymbol{g}$ parameter characterizing free electrons. We believe that this line is attributable to free radicals.

3.2.3. Analysis of the temperature dependence of EPR spectra

The small value of root mean sum of squares of weighted differences between the observed and calculated resonance line positions (RMSD) [22] only indirectly confirms the model of the Yb^{3+}/Er^{3+} ion pairs in the LN crystal. Therefore, an additional confirmation of the adopted model is required, e.g. by deconvolution of the main fine transitions and the temperature dependence of the total EPR line intensity.

3.2.3.1. LN:Yb. The EPR spectra obtained in the temperature range from 6.5 K to 41 K at a fixed angle ($\theta = 10°$) in the *ZY* plane are presented in Fig. 8. A strong line centered at about 165 (mT) (line 1, indicated by the left arrow) and a very strong line centered at about 200 (mT) (line 2, indicated by the right arrow) are recognizable, the best visible lines in the top EPR spectrum ($T = 6.5$ K). The EPR line intensity and the inverse intensity are shown in Fig. 9. The EPR line intensity was computed as the product of the square of the line's width and height. The EPR line intensity as a function of temperature (see Fig. 9, upper panel) indicates that line 2 is much stronger than line 1, even though the two curves are shown in different scales. With decreasing temperature, the EPR line intensity of each line increases non-linearly.

The sudden change in the EPR line intensity for line 2 can be observed between 7 K and 7.4 K. A similar variation, though considerably more moderate, is observable in the temperature dependence

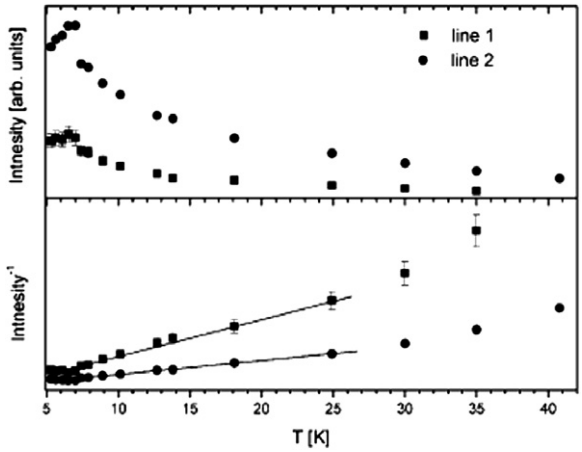

Fig. 9. Temperature dependence of the EPR line intensity (top panel, different scale applied to each curve) and the inverse intensity (bottom panel) measured at a fixed angle ($\theta = 10°$) in the *ZY* plane containing the crystal's *c*-axis: line 1 – solid squares, line 2 – solid dots. Experimental uncertainty indicated by the error bars is much less than the size of data points.

of the EPR line intensity of line 1. It follows from Fig. 9 (bottom panel) that the temperature dependence of the inverse intensity for each line is well described by a linear approximation in the temperature range from ~25 K to ~7 K. This indicates that the Curie–Weiss law is well obeyed for both lines in this temperature range. However, linear approximation yields essentially different model parameters for the two lines.

The shape of the main EPR line 2 changes with temperature, suggesting that the line may be a superposition of several lines arising from different paramagnetic centers. In order to describe the line's asymmetrical shape, we tentatively adopted three Lorentz lines, 2a, 2b and 2c, a reasonable minimum number of lines in a deconvolution.

The deconvolution of EPR line 2 into its three constituent lines, 2a, 2b and 2c, is shown in Fig. 10. The sum of the constituent lines reflects the shape of line 2 very well, which confirms the correctness of our approach.

The temperature dependence of intensity is shown in Fig. 11 for each of the three deconvoluted lines. The intensity of EPR line 2 turns out to be dominated by the intensity of line 2b. The intensity

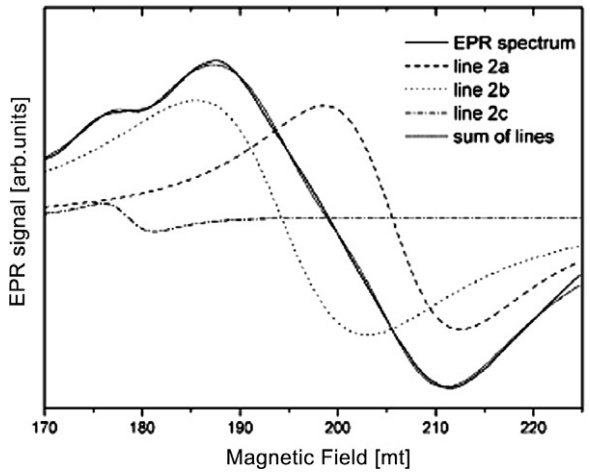

Fig. 10. Deconvolution of EPR line 2 at $T = 12.7$ K into three constituent lines, 2a, 2b and 2c.

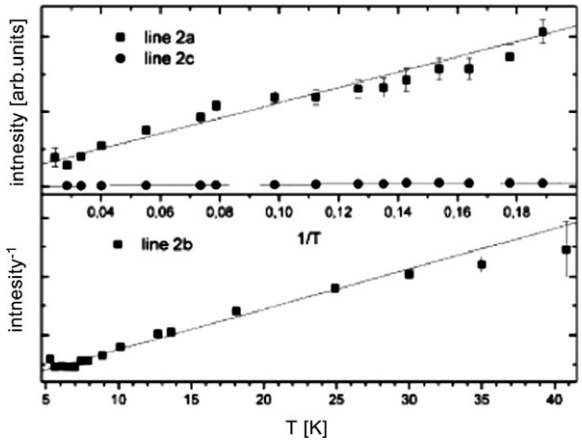

Fig. 12. Dependences of (i) the intensity of deconvoluted lines 2a and 2c on $1/T$ (top panel) and (ii) the inverse intensity of deconvoluted line 2b on T (bottom panel); solid lines obtained by linear fitting using the Curie or Curie–Weiss law.

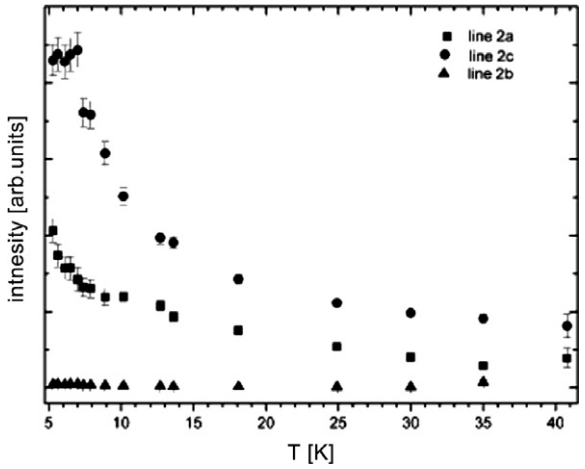

Fig. 11. The temperature dependence of line intensity for deconvoluted lines 2a, 2b and 2c.

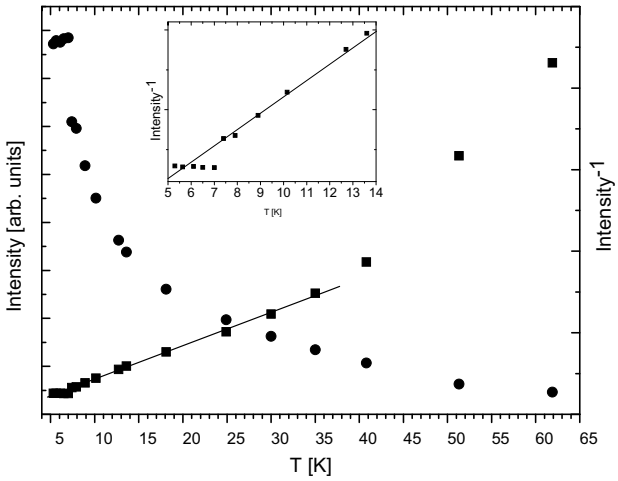

Fig. 13. The temperature dependences of the total EPR line intensity of LN:Yb (left axis, solid dots) and its inverse (right axis, solid squares); experimental uncertainty is less than the size of data points. Inset is an enlarged section of the inverse intensity's low temperature dependence revealing unusual divergence from the Curie–Weiss law.

of line 2c (see Fig. 11, solid triangles) increases very weakly with decreasing temperature, while that of line 2a (see Fig. 11, solid squares) increases. The intensity of line 2b (see Fig. 11, solid circles) increases with decreasing temperature and additionally exhibits a sudden increase at about 7.2 ± 0.2 K, followed by a flattened decrease below this temperature. This disparate behavior of the three constituent lines indicates that line 2b originates from other paramagnetic centers than lines 2a and 2c.

The top panel of Fig. 12 shows the dependence of the intensity of lines 2a and 2c versus $1/T$, whereas the bottom panel presents the inverse intensity of line 2b versus T. The best fitted results (solid lines) obtained using linear fitting based on the Curie or Curie–Weiss law are included.

At a temperature of 12.7 K (deconvoluted line), the intensity of the EPR line turns out to be dominated by the intensity of one of the three lines (line 2b in Fig. 12), exhibiting the Curie–Weiss behavior responsible for pairs of Yb^{3+} ions. The other two lines – 2a and 2c in Fig. 12 – exhibit the Curie behavior and may be ascribed to isolated Yb^{3+} ions.

Let us now consider the temperature dependence of the total EPR line intensity and its inverse at a fixed angle of $\Theta = 10°$, as shown in Fig. 13. The total intensity is calculated using double numerical integration of the EPR signal [19], which reveals the same behavior as the above-mentioned line 2, predominant in the EPR spectra (see Fig. 10). However, significant differences appear at temperatures above 30 K. Two distinct regions can be identified in the total inverse intensity diagram (solid squares): (i) a low temperature region between 5 K and 40 K and (ii) a higher temperature region between 40 K and 62 K, where the EPR lines disappear. In both regions, the total inverse intensity versus T may be described well enough by the Curie–Weiss law, which enables us to determine the constant $\Theta = -0.6 \pm 0.3$ K. The negative Θ suggests that antiferromagnetic interactions may occur in the system of Yb^{3+} ions in LN. The temperature behavior of the total intensity and its inverse may be explained by the presence of antiferromagnetically coupled Yb^{3+} ion pairs in LN crystal, thus confirming the conclusion from our earlier EPR and optical measurements [13,22].

The EPR lines observed in the low temperature region arise predominantly from Yb^{3+} centers (pairs of ytterbium ions dominate up to about 12 K). Above 40 K, these EPR lines vanish and other lines appear, of very low intensity. The origin of these lines is not clear at the moment, possibly attributable to some dopant paramagnetic ions entering the LN structure as impurities from chemical ingredients during the crystals' growth.

3.2.3.2. LN:Er. As the main EPR line of LN:Er (sample #5) shown in Fig. 3 changes its shape depending on temperature, it appears to be a superposition of two or more paramagnetic centers, as in the case of the LN:Yb crystal,. The linewidth of the main EPR line is about 2 mT. As the results of deconvolution of a narrow line into several lines were not satisfactory, we deconvoluted the EPR line into 2 Lorentzian-shaped lines.

An exemplary deconvolution of the central EPR line corresponding to the fine-structure transition of ^{even}Er ions obtained at $T = 6.3$ K is shown in Fig. 14. The EPR spectrum is shown as a solid line, the two constituent lines are dashed and their sum is a dotted line. Good agreement between the experimental EPR spectrum and the sum of the two constituent Lorentz-shaped lines (see Fig. 14) is notable.

The temperature dependence of the width and intensity of the two constituent lines are shown in Fig. 15. The line marked as 2 (solid squares) is dominant at temperatures above ~25 K, whereas below 25 K the intensity and line width of the EPR spectrum are dominated by line 1 (solid circles). Line 1 suddenly decreases in intensity and increases in line width at temperatures below 4.5 K (see Fig. 15, bottom panel). Line 1 may be ascribed to the paramagnetic centers originating from $^{even}Er^{3+}$–$^{even}Er^{3+}$ ion pairs, while line 2 corresponds to paramagnetic centers originating from isolated $^{even}Er^{3+}$ ions.

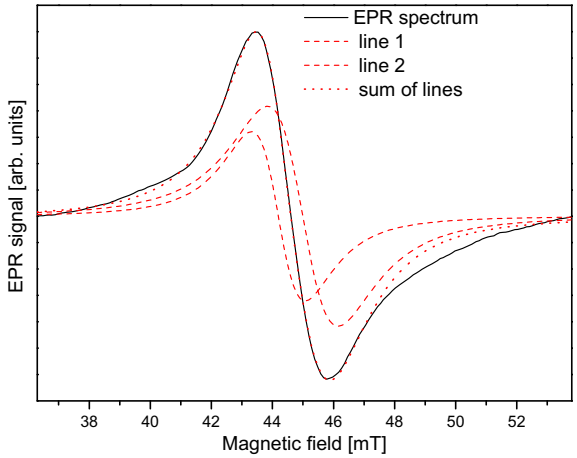

Fig. 14. Sample deconvolution of the EPR line at $T = 6.3$ K: the EPR spectrum (solid line), the two constituent lines (dashed) and their sum (dotted line).

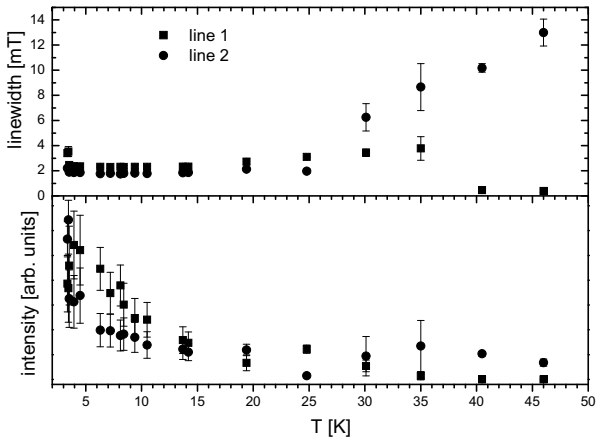

Fig. 15. The temperature dependences of line width (top panel) and intensity (bottom panel) for deconvoluted lines 1 and 2 of LN:Er, respectively marked as solid squares and circles.

Let us now consider the temperature dependence of the total EPR line intensity and its inverse for a LN:Er sample oriented so that the magnetic field is parallel to the *z*-axis (optical *c*-axis). The temperature dependences of the intensity and width of the main EPR line originating from ^{even}Er ions are presented in Fig. 16. The total intensity of the main EPR line initially increases with decreasing temperature, reaches a maximum at the temperature of $T = 4.5$ K and decreases at lower temperatures. The decrease is not linear; it rather resembles a bump in the temperature range between 3.36 K and 4.5 K. Such behavior of the total intensity of EPR lines is characteristic for pairs of ions. Lastly, the total intensity and width of the EPR line increase above the temperature of ~35 K.

This is a surprising phenomenon, as the intensity of EPR lines originating from RE ions should decrease with increasing temperature and vanish in this temperature range. As in the case of the LN:Yb crystal, we suppose that it may be due to paramagnetic ions entering the LN structure as uncontrolled impurities from chemical ingredients during the crystal growth process. So, this is the same conclusion we have made.

The temperature dependence of the EPR line's inverse intensity is shown in Fig. 17. Generally speaking, two distinct regions can be identified: a low temperature region between 3 K and

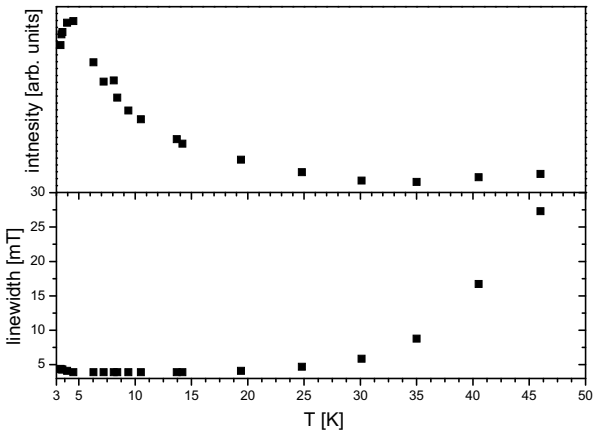

Fig. 16. The temperature dependences of the total intensity (top panel) and width (bottom panel) of the main EPR line of an LN:Er^{3+} single crystal.

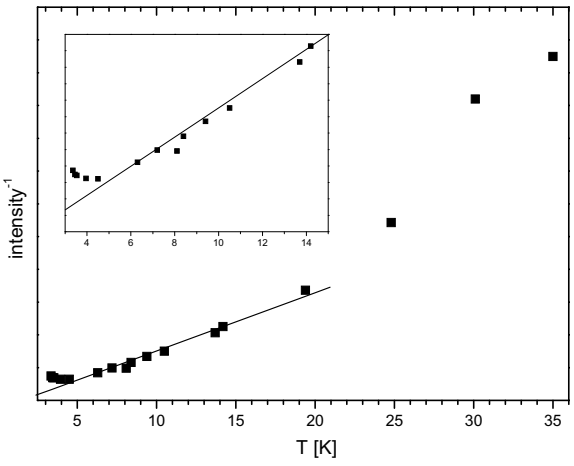

Fig. 17. Temperature dependence of the inverse intensity of the EPR line of an LN:Er^{3+} single crystal measured in magnetic field parallel to the crystal's *Z* (optical *c*) axis; experimental uncertainty indicated by error bars is much less than the size of data points. Inset is an enlarged section of the low temperature dependence (below 15 K).

~20 K and a high temperature region above 20 K. In the low temperature region, the total inverse intensity versus T may be described well enough by the Curie–Weiss law, save for the very low temperature region below 4.5 K, which exhibits an apparent departure from the Curie–Weiss law (see inset in Fig. 17). This allows us to determine the Curie–Weiss constant at $\Theta = 1.5 \pm 0.5$ K. The constant's positive sign suggests that the ferromagnetic interactions arise in the system of $^{even}Er^{3+}$–$^{even}Er^{3+}$ ion pairs in LN.

The temperature dependence of the intensity and inverse intensity of the main EPR line measured in the LN:Er sample is explicable by superposition of several resonance lines originating from isolated $^{even}Er^{3+}$ ions and/or $^{even}Er^{3+}$–$^{even}Er^{3+}$ ion pairs. The sharp increase in the EPR line's intensity near the maximum at $T = 4.5$ K, followed by a decrease with decreasing temperature, and the linear increase of the inverse intensity in the same temperature region indicate that the main EPR line below 20 K is dominated by signals originating from $^{even}Er^{3+}$–$^{even}Er^{3+}$ ion pairs. Above 20 K, the resonance signal originating from $^{even}Er^{3+}$–$^{even}Er^{3+}$ ion pairs disappears quickly, followed by an EPR line dominated by a signal arising from isolated $^{even}Er^{3+}$ ions. This signal vanishes above 35 K and the EPR line reveals an additional resonance signal originating from paramagnetic centers of uncertain origin.

We can conclude that our analysis of the temperature dependence of the intensity and width of the main EPR line has confirmed our previous conclusions from optical measurements and the results of deconvolution of the main EPR line.

3.3. Non-equivalent crystallographic sites of low C_1 point group symmetry

Apart from isolated and paired paramagnetic centers, changing intensity of EPR lines versus temperature may also be related to the presence of several non-equivalent crystallographic centers of isolated Er^{3+}/Yb^{3+} ions in an LN single crystal.

The crystallographic arrangement of constituent atoms of an LN crystal projected on the (0001) plane (perpendicular to the c-axis) is shown in Fig. 18, with oxygen octahedra around impurity ions marked as large spheres. If an Er^{3+}/Yb^{3+} ion is incorporated into a Li^+ site (the small sphere in the center), charge compensation is required, achievable with cation vacancies occurring in the impurity ion's vicinity. The local site symmetry of paramagnetic Er^{3+}/Yb^{3+} centers may be either C_1 or C_3 (axial) [4,26]. Having observed new low symmetry C_1 centers [11,22] in LN:Yb single crystals, we focused on the crystallographically inequivalent C_1 sites. Six possible vacancies in the first shell are marked in Fig. 18: Li^+ vacancies 1, 2, 3 and Nb^{5+} vacancies 1′, 2′, 3′. However, this appears to have been a mistake. The distance between Yb^{3+} and Nb^{5+} ions is equal to 0.3062 nm and 0.3363 nm, respectively for the 1, 2, 3 and 1′, 2′, 3′ ions. The distance to Li^+ sites, above or below the plane with the Er^{3+}/Yb^{3+} ion, is 0.3765 nm. In fact, there are six Nb^{5+} sites in the first shell and six Li^+ sites in the second shell in the plane containing the Er^{3+}/Yb^{3+} ion. As each Nb^{5+} ion in positions 1–6 is connected to an Er/Yb_{Li} ion with an O^{2-} bridge, cation vacancies in the first shell tilt the Er^{3+}/Yb^{3+} $\boldsymbol{g}$ tensor and reduce the local site symmetry of Er^{3+}/Yb^{3+} ions. Reduced symmetry of a dopant ion may also be due to its off-centered actual position, violating the inverse symmetry inside its first shell. Thus, we can identify six NEC Er/Yb_{Li}–V_i paramagnetic centers (erbium/ytterbium at Li positions connected with one of V_i vacancies, $i = 1$–6) exhibiting low C_1 symmetry, expected to dominate the EPR spectrum. As shown in Fig. 18, all Er/Yb_{Li}–V_i centers have the same surroundings, so their EPR line shapes should exhibit the same thermal behavior, i.e. the temperature dependence of the intensity of EPR lines originating from these centers should behave similarly. We can conclude that the change in the intensity of the EPR lines versus temperature cannot be related to the existence of several non-equivalent crystallographic sites (NEC) of single Er^{3+}/Yb^{3+} ions in our samples of lithium niobate doped with erbium or ytterbium.

Fig. 18 could also provide a model of Er^{3+}/Yb^{3+}–Er^{3+}/Yb^{3+} ion pairs in LN:Er/Yb single crystals, in which one Er^{3+}/Yb^{3+} ion is incorporated into a Li^+ site and the other – into a Nb^{5+} site in the first shell (positions 1, 2, 3, 1′, 2′ and 3′). All these paramagnetic centers should display C_1 symmetry.

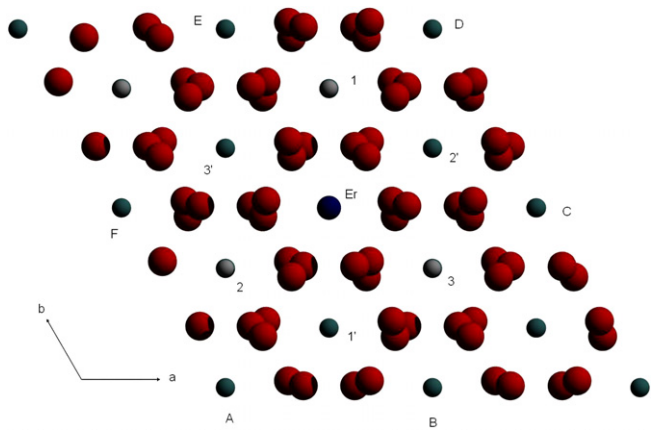

Fig. 18. Crystallographic arrangement of constituent atoms of an LN:Er crystal projected on the (0001) plane (perpendicular to the c-axis): Er – substitution for Li^+, 1, 2, 3 – Li^+ sites in the first shell below the Er ion, 1′, 2′, 3′ – Nb^{5+} site in the first shell above the Er ion, A, B, C, D, E, F – Li^+ in the second shell in the plane contain Er, large spheres – O^{2-} ions.

4. Conclusions

Optical absorption measurements of the investigated crystals suggest the presence of localized phonons. The Raman spectra provide similar indications as the optical studies. The localized phonons may be considered as indirect evidence of local perturbations around Er/Yb ions, possibly due to the formation of Er/Yb–Er/Yb ion pairs.

The angular dependence of the EPR lines of the LN:Yb single crystal exhibit behavior characteristic for sites of very low symmetry. When the magnetic field's direction rotates away from the z-axis, the lines move towards higher magnetic field values. The EPR spectra are interpreted using a spin Hamiltonian for dissimilar Yb^{3+} ion pairs. This model yields overall agreement of the experimental line positions with the simulated results and explains the observed spectral features, apparently attributable to the C_1 symmetry of Yb ions.

The temperature behavior of the EPR line's intensity and its inverse for LN:Yb single crystals indicates that at about 8 K signals appear in the spectra that can be ascribed to antiferromagnetically coupled Yb^{3+} ion pairs of dissimilar ions in the LN crystal, i.e. $^{even}Yb^{3+}$–$^{even}Yb^{3+}$ pairs of different g_{ij} values, probably located at the neighboring (closest) Li^+ and Nb^{5+} positions. The EPR line intensity obeys the Curie–Weiss law and yields the antiferromagnetic interaction constant of $\Theta = -0.6 \pm 0.3$ K. Yb^{3+} ions dominate the temperature dependence of EPR line intensity up to 40 K. Above this temperature, EPR lines characteristic for Yb^{3+} ions disappear and new lines appear, attributable to some dopant paramagnetic ions entering the LN structure as impurities from chemical ingredients during the crystal's growth.

After deconvolution of the main EPR line into several Lorentzian components, the Er^{3+} center with the lowest C_1 point group symmetry was resolved and values of the $\boldsymbol{g}$ – tensor were estimated in the angular dependence of the EPR spectra of the LN:Er^{3+} crystal.

The temperature dependences of the EPR line intensity and the inverse intensity of the main EPR line of LN:Er single crystals is explicable by assuming that the EPR line is a superposition of several paramagnetic centers originating from isolated $^{even}Er^{3+}$ ions and $^{even}Er^{3+}$–$^{even}Er^{3+}$ ion pair. At temperatures below 20 K, the main EPR line is dominated by signals from $^{even}Er^{3+}$–$^{even}Er^{3+}$ ion pairs and satisfies the Curie–Weiss law, $\Theta = 1.5 \pm 0.5$ K, indicating ferromagnetic interactions between erbium ions. Above 20 K, the resonance signal is dominated by a signal originating from isolated $^{even}Er^{3+}$ ions. Above 35 K, an additional EPR resonance signal appears originating from unknown paramagnetic centers, possibly accidental impurities.

The presence of accidental impurities may promote the process of Er(Yb) cluster formation in congruent lithium niobate host crystals.

Crystallographic analysis has excluded the possibility that the temperature behavior of the EPR line's intensity could be related to the existence of several inequivalent crystallographic sites of isolated Yb(Er) ions in a LN:Yb(Er) single crystal.

The combined indications from the optical and EPR spectroscopy measurements suggests the existence of Er^{3+}/Yb^{3+}–Er^{3+}/Yb^{3+} ion pairs in our weakly doped LN:Er^{3+}/Yb^{3+} single crystals with high probability. Our results suggest that EPR signals could also be interpreted as originating from coupled paramagnetic centers, even in the case of weakly doped single crystals.

Acknowledgments

The authors would like to thank Professor Taiju Tsuboi from Kyoto Sangyo University, Japan, for low temperature absorption measurements. They also gratefully acknowledge a DSc (habilitation) grant for T. Bodziony and a Professorial grant for S.M. Kaczmarek, both from the SUT.

References

[1] J.M. Cabrera, J. Olivares, M. Carrascosa, J. Ramis, R. Muller, E. Dieguez, Adv. Phys. 45 (1996) 349.
[2] Properties of Lithium Niobate, 1989 Inspec, EMIS Datareviews Series No. 5.
[3] S.C. Abrahams, J.M. Reddy, J.L. Bernstein, J. Phys. Chem. Solids 27 (1966) 997.
[4] G. Malovichko, V. Grachev, V. Kokanyan, O. Shirmer, Phys. Rev. B 59 (1999) 9113.
[5] G. Burns, D.F. O'Kane, R.S. Title, Phys. Rev. 167 (1968) 314.
[6] C. Bonardi, C.J. Magon, E.A. Vidoto, M.C. Terrile, L.F. Bausa, E. Montoya, D. Bravo, A. Martin, F.J. Lopez, J. Alloys Compd. 323&324 (2001) 340.
[7] S.H. Choh, J.H. Kim, I.W. Park, H.J. Kim, D. Choi, S.S. Kim, Appl. Magn. Reson. 24 (2003) 313.
[8] J. Amin, B. Dussardier, T. Schweizer, M. Hempstead, J. Lumin. 69 (1996) 17.
[9] V. Dietrolf, M. Koerdt, Phys. Rev. B 61 (2000) 80.
[10] D.M.B.P. Milori, I.J. Moraes, A.C. Hernandes, R.R. de Souza, M. Siu Li, M.C. Terrile, Phys. Rev. B 51 (1995) 3206.
[11] T. Bodziony, S.M. Kaczmarek, Opt. Mater. 29 (2007) 1440.
[12] T. Bodziony, S.M. Kaczmarek, Physica B 400 (2007) 95.
[13] T. Bodziony, S.M. Kaczmarek, J. Hanuza, J. Alloys Compd. doi:10.1016/j.jallcom.
[14] I. Pracka, M. Malinowski, A.L. Bajor, B. Surma, Z. Gałązka, M. Świrkowicz, M. Możdżonek, Proc. SPIE 3178 (1997) 295.
[15] T. Tsuboi, S.M. Kaczmarek, G. Boulon, J. Alloys Compd. 380 (2004) 196.
[16] A. Lorenzo, H. Loro, J.E. Munoz Santistute, M.C. Terrile, G. Boulon, J. Garcia Sole, Opt. Mater. 8 (1997) 55.
[17] S.M. Kaczmarek, T. Tsuboi, M. Ito, G. Boulon, G. Leniec, J. Phys. Condens. Matter 17 (2005) 3771.
[18] R. Mouras, P. Bourson, M.D. Fontana, G. Boulon, Opt. Commun. 197 (2001) 439.
[19] A. Abragam, B. Bleaney, Electron Paramagnetic Resonance of Transition Ions, Clarendon, Oxford, 1970.
[20] O. Guillot-Noel, P. Goldner, P. Higel, D. Gournier, J. Phys. Condens. Matter 16 (2004) R1.
[21] A. Bencini, D. Gatteschi, Electron Paramagnetic Resonance of Exchange Coupled Systems, Springer, Berlin, 1990.
[22] T. Bodziony, S.M. Kaczmarek, Res. Chem. Intermediates 33 (8–9) (2007) 885.
[23] J.R. Pilbrow, Transition Ion Electron Paramagnetic Resonance, Clarendon, Oxford, 1990.
[24] D.G. McGavin, M.Y. Mombourquette, J.A. Weil, Computer Program EPR–NMR, Version 6.5, Department of Chemistry, University of Saskatchewan, Saskatoon, Canada, 2002.
[25] G. Malovichko, V. Grachev, S. Okulov, E. Kokanyan, F. Henecker, A. Hofstaetter, O. Shirmer, Phys. Status Solidi (b) 243 (2006) 409.
[26] Th. Nolte, Th. Pawlik, J.M. Spaeth, Solid State Commun. 104 (1997) 535.